Electronic Supplementary Material (ESI) for Journal of Materials Chemistry A.

Supplementary Information

Photo-induced Au-Pd Alloying at TiO_2 {101} Facets Enables Robust CO_2 Photocatalytic Reduction into Hydrocarbon Fuels

Qian Chen,[a] Xianjie Chen,[b] Minling Fang, [a] Jiayu Chen,[a] Yongjian Li,[a] Zhaoxiong Xie,[a] Qin Kuang,*[a] Lansun Zheng[a]

Corresponding Author

*E-mail: qkuang@xmu.edu.cn

1. Experimental Procedure

Chemicals and Regents

Degussa P25 was purchased from Shanghai Haiyi Co., Ltd. Potassium hydroxide (KOH, 90%), hexamethylenetetramine (HMTA, 99%), L-ascorbic acid (AA, AR), methanol (CH_3OH, AR), tetrachloroauric (III) acid tetrahydrate ($HAuCl_4 \cdot 4H_2O$, AR) and isopropyl alcohol (IPA, AR) were received from Sinopharm Chemical Reagent Co., Ltd. Sodium tetrachloropalladate (II) (Na_2PdCl_4, 98%) was received from Kunming Institute of Precious Metals. Polyvinylpyrrolidone (PVP, MW=8000, AR) were obtained from Alfa Aesar Co., Ltd. All chemicals and regents were used as received without further treatment. Ultrapure water was used in all experiments.

Synthesis of Anatase TiO_2 with Exposed {101} and {001} Facets

{101} and {001} facets co-exposed TiO_2 nanocrystals (NCs) were synthesized via a two-step hydrothermal reaction reported by our group.[1, 2] Firstly, Degussa P25 (2.0 g) and KOH (44.8 g) were dispersed in ultrapure water (80 mL) and stirring for 30 min under room temperature. The mixture was divided into three equal parts and transferred to three 50 mL Teflon-lined autoclaves, followed by the hydrothermal treatment at 200 °C for 24 h. The resultant potassium titanate nanowires (KTNWs) were washed and centrifuged with ultrapure water until the supernatant showed neutrality. Secondly, anatase TiO_2 with exposed {101} and {001} facets were prepared by using KTNWs and HMTA as precursor and shape regulator, respectively. Typically, KTNWs (10 mg) were dispersed in ultrapure water (3 mL) to form a white suspension under intense ultrasonic treatment over 30 min. HMTA (2.1 g) dissolved in ultrapure water (3 mL) were added into above white suspension and vigorously stirred for another 30 min. The mixture was transferred to 25 mL Teflon-lined autoclaves and was kept at 200 °C for 12 h. Finally, the target TiO_2 was collected by successive washing and drying procedures.

Deposition of Au-Pd Alloy Nanoparticles (NPs) on TiO_2 Facets

Non-selective deposition on {101} and {001} facets

Au-Pd alloy NPs (total mass fraction of Au and Pd =1wt %, Au/Pd molar ratio of 1:1) were synthesized and supported on TiO_2 via chemical reduction method by using AA as reducing agent. TiO_2 powder (20 mg), PVP (30 mg) and AA (80 mg) were dispersed in ultrapure water (20 mL) after an ultrasonic treatment for 10 min to form a homogeneous mixture. To this suspension were added dropwise the desired volume of $HAuCl_4$ (1g L^{-1}) and Na_2PdCl_4 (1g L^{-1}) mixed solution (See Table S1 for volume details of $HAuCl_4$ and Na_2PdCl_4 solutions), followed by stirring in a 60 °C water bath for 4 h. Finally, the samples were washed with ethanol and water for several times and dried in a vacuum oven overnight.

Selective Deposition on {001} Facets

For realizing the selective deposition of Au-Pd alloy (total mass fraction of Au and Pd =1wt %，Au/Pd molar ratio of 1:1) on {101} facets, photo-irradiation reduction was conducted in this experiment segment. Typically, TiO_2 powder (20 mg) and PVP (30 mg) was ultrasonic dispersed in methanol solution (30 mL, 30 vol %), followed by the injection of desired volume of $HAuCl_4$ (1g L^{-1}) and Na_2PdCl_4 (1g L^{-1}) mixed solution. Then, the slurry underwent an UV light irradiation set-up (average light density 5.3 mW cm^{-2}) under room temperature for 2 h to complete this reduction process. Finally, the samples were washed with ethanol and water for several times and dried in a vacuum oven overnight. In order to synthesize AuPd alloy with various element molar ratio, different volumes of Au and Pd precursors were employed with fixing the total metal mass percentage of ~1 wt. % for both mono- and bi-metallic Au-Pd loaded TiO_2 (See Table S1 for volume details of $HAuCl_4$ and Na_2PdCl_4 solutions).

Characterizations of Materials

The surface morphologies of as-prepared TiO_2 were characterized by a scanning electron microscope (SEM, Hitachi S-4800). All samples for the TEM analysis were investigated on a transmission electron microscope (TEM, Hitachi 7700) and a high resolution transmission electron microscope (HR-TEM, JEM 2010E) with an accelerating voltage of 200 kV. The high-angle annular dark-field scanning transmission electron microscopy (HAADF-STEM) and energy dispersive X-ray spectroscopy (EDX) elemental mapping were performed with a FEI TECNAI F30 microscope operated at 300 kV. The crystal phase of products was determined by powder X-ray diffraction (XRD) using a Rigaku Ultima IV X-ray diffractometer with Cu Kα radiation. Mass spectrometer (MS, Agilent 5975c) was employed to confirm the carbon source of hydrocarbons, by using $^{13}CO_2$ (Sigma-Aldrich, 99% atom ^{13}C) as feeding gas. The surface states and chemical compositions of products were analysed using X-ray photoelectron spectroscope (XPS, ESCALAB 250Xi, Thermo Scientific). All binding energies were calibrated using the contaminant carbon (C1s= 284.6 eV). UV–visible diffuse reflectance spectra (UV-Vis DRS) were obtained on a Hitachi U-3010 UV-vis spectrophotometer with $BaSO_4$ as reference. The steady state photoluminescence (PL) and time resolved photoluminescence (TR-PL) spectra were recorded by utilizing the fluorescence spectrophotometer (Edinburgh, FLSP920) with an excitation wavelength of 230 nm under room temperature. Surface photovoltage (SPV) spectroscopy was recorded on a self-made instrument, with the raw data normalized by an illuminometer (Zolix UOM-1S). CO_2 adsorption isotherms were collected on a Micrometrics (ASAP 2010V5.02H) surface area analyser. The samples were degassed in vacuum at 120 °C for 12 h and then measured in 0 °C ice-water bath. *In situ* diffuse reflectance infrared Fourier transform spectroscopy (DRIFTS) was tested on an infrared spectrometer (BRUKER VERTEX 70), in which a 300 W Xe lamp was employed as light source. The baselines are

deducted from all spectra to exclude environment factors, and the bands of KBr in the presence of CO_2 and water vapor under light irradiation are set as reference. The actual mass fractions of Au and Pd elements in the composite photocatalysts were determined by inductively coupled plasma atomic emission spectrometry (ICP-AES, Baird PS-4).

Photoelectrochemical Measurements

Photoelectrochemical properties of samples were investigated on an electrochemical workstation (CHI-660D, China) equipped with three-electrode system. In a typical experiment, a platinum wire and saturated calomel electrode were employed as counter electrode and reference electrode, respectively. A 300 W Xe lamp was utilized as the light source. CO_2 saturated $NaHCO_3$ aqueous solution (0.1 mol L^{-1}) was served as electrolyte. For the fabrication of working electrode, photocatalyst (10 mg) was homogeneously dispersed in isopropyl alcohol (1 mL). The suspension was drop-coating on an indium tin oxide conducting (ITO) glass and naturally dried under ambient condition. The transient photocurrent responses were obtained under Xe lamp with the light chopped manually at regular intervals. Linear sweep voltammetry (LSV) with a scan rate of 10 mV s^{-1} were measured under uninterrupted irradiation.

Photocatalytic CO_2 Reduction

The CO_2 photoreduction was carried out in a commercial evaluation system equipped with a quartz cell (total volume of 150 mL) via vapor-solid reaction mode. Powder photocatalyst (10 mg) was sampled and evenly coated on a piece of quartz plate (2.5*3.5 cm^2). This plate was intentionally pretreated in a long-term vacuum drying process (150 °C, 12 h) and UV light irradiation (light intensity of 5.3 mW cm^{-2}) for 2 h to remove the residual water and organic contaminants, respectively. This plate was vertically placed in the reaction cell. Ultra-pure water (0.1 mL) as proton source was injected into quartz cell. Then entire reaction setup was sealed and

vacuum degassed for several times, followed by high-purity CO_2 filled into the reactor to reach a pressure at 0.26 MPa. Prior to light illumination (300 W Xe lamp, light intensity of 853 mW cm^{-2}), the reactor stored in dark was heated to 40 °C accompanied by continuously stirring for 1 h to ensure an adsorption-desorption equilibrium of CO_2 and aqueous vapor over photocatalysts. The gas-phase products were collected every hour and analyzed online by gas chromatography (KE CHUANG GC 2002, China). Argon (Ar) gas was used as carrier gas. The amounts of hydrocarbons were determined using a flame ionization detector (FID). Carbon monoxide (CO) was converted to methane (CH_4) in methanation reactor and then detected by FID. The amount of hydrogen (H_2) was analyzed via a thermal conductivity detector (TCD). To evaluate the efficiency of CO_2 reduction, we can calculate the selectivity (Sel.) by adding up the reacted electrons towards specific reduction products[3] as follows:

Equation S1:

$$Sel.\ of\ hydrocarbons = \frac{n(CH_4) * 8 + n(C_2H_4) * 12 + n(C_2H_6) * 14}{n(CH_4) * 8 + n(C_2H_4) * 12 + n(C_2H_6) * 14 + n(CO) * 2 + n(H_2) * 2}$$

2. Supplementary results and discussion

Table S1. The detailed volume of $HAuCl_4$ and Na_2PdCl_4 solutions in preparing samples.

Samples	$HAuCl_4$(v/uL)	Na_2PdCl_4(v/uL)
CR-Au_1Pd_1	270	194
PD-Au	418	0
PD-Au_8Pd_1	395	30.5
PD-Au_6Pd_1	382	45.8
PD-Au_4Pd_1	368	66
PD-Au_2Pd_1	330	117
PD-Au_1Pd_1	270	194
PD-Au_1Pd_4	132	378
PD-Pd	0	555

Table S2. ICP-AES results of as-prepared samples.

Samples	Noble metal elements (/ wt. %)			Molar ratio (n_{Au}: n_{Pd})
	Au	Pd	Au + Pd	
CR-Au_1Pd_1	0.65	0.33	0.98	1.05
PD-Au	0.95		0.95	
PD-Au_8Pd_1	0.94	0.06	1.00	8.51
PD-Au_6Pd_1	0.89	0.09	0.98	5.41
PD-Au_4Pd_1	0.87	0.12	0.99	3.83
PD-Au_2Pd_1	0.78	0.20	0.98	2.05
PD-Au_1Pd_1	0.62	0.33	0.95	1.02
PD-Au_1Pd_4	0.30	0.68	0.98	0.24
PD-Pd		0.97	0.97	

Table S3. Summary of noble metal(s)/TiO_2 materials for photocatalytic CO_2 reduction under similar catalytic conditions.

Photocatalysts	Reduction products (μmol g^{-1} h^{-1})					Sel. of hydrocarbons [a]	References
	CH_4	C_2H_4	C_2H_6	CO	H_2		
PD-Au_6Pd_1	**12.7**	**0.7**	**0.8**	**10.9**	**0**	**85%**	**This work**
Au-Pd/3DOM-TiO_2	18.5	0	0	1.2	18.6	79%	(4)[4]
Au/PC500 TiO_2	8	0	1	2	9.5	77%	(5)[5]
$PdH_{0.43}$/TiO_2 nanosheets	20.5	0	0	4.5	45	62%	(6)[6]
Cu/Pt/TiO_2-5h	33	0	0	8.3	25	80%	(7)[7]
3.0% MgO−Pt−TiO_2	6.3	0	0	0.02	5.1	83%	(9)[8]
0.5Pt/TiO_2-COK-12	10.6	0	0	0	55.56	43%	(8)[9]
Au@TiO_2-20-Au	0.833	0	0	0.67	8.33	27%	(10)[10]

[a] The sel. of hydrocarbons was calculated by adding up the reacted electrons towards specific reduction products as follows:

Equation S1:

$$Sel.\ of\ hydrocarbons = \frac{n(CH_4) * 8 + n(C_2H_4) * 12 + n(C_2H_6) * 14}{n(CH_4) * 8 + n(C_2H_4) * 12 + n(C_2H_6) * 14 + n(CO) * 2 + n(H_2) * 2}$$

As shown is Table S3, through the comparison with those noble metal(s)/TiO_2-based photocatalysts under similar catalytic conditions reported by literatures, our as-prepared PD-Au_6Pd_1 shows advantages in the following three aspects: (i) the higher sel. of hydrocarbons fuels, (ii) the obviously suppressed side reaction, such as hydrogen evolution, and (iii) a certain amount of C_2H_4 and C_2H_6 were detected, but rare in the references cited above.

Table S4. A examine of photogenerated electron-hole balance in PD-Au_6Pd_1.

	Reduction products				Oxidation products	Electron-hole balance [a]
Evolution rate	CH_4	CO	C_2H_4	C_2H_6	O_2	N_{e^-}/N_{h^+}
(μmol g^{-1} h^{-1})	12.78	10.76	0.73	0.79	35.36	1.02

[a] The electron-hole balance was evaluated by the ratio of [$8n(CH_4) + 2n(CO) + 12n(C_2H_4) + 14n(C_2H_6)$] amounts to [$4n(O_2)$] amounts.

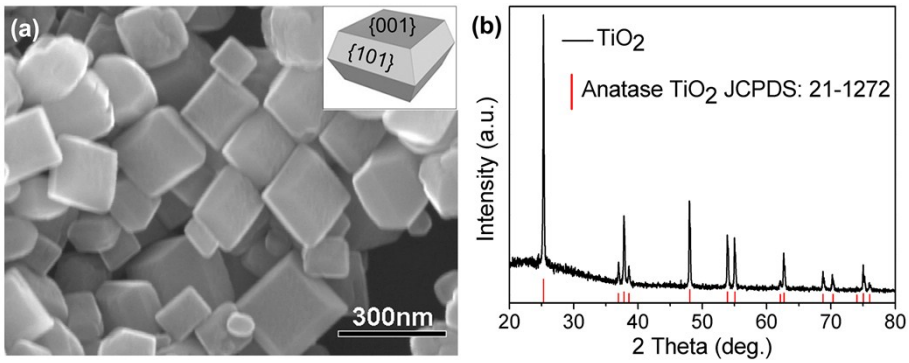

Figure S1. (a) SEM image and the corresponding structural model (Insets) and (b) XRD pattern of {101} and {001} facets co-exposed TiO_2.

As shown in Figure S1a, the as-prepared TiO_2 are enclosed by two {001} on the top/bottom and eight {101} facets on the side surface, exhibiting a well-defined truncated tetragonal bipyramidal morphology. The corresponding XRD pattern (Figure S1b) indicates the pure anatase phase TiO_2 (JCPDS *no.* 21-1272) without any other impurities can be obtained in this case.

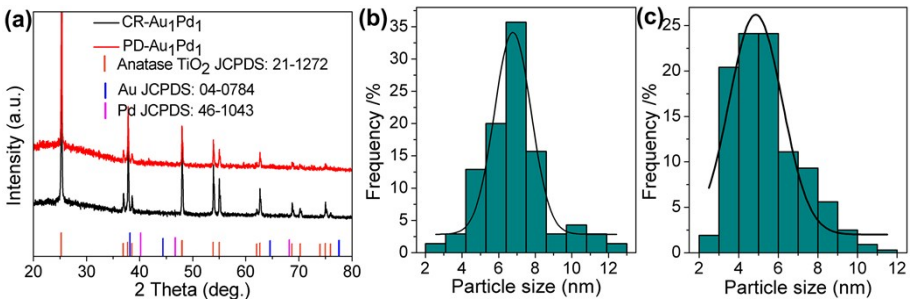

Figure S2. (a) XRD pattern and the size distribution of Au-Pd alloy particles loaded on (b) CR-Au_1Pd_1 and (c) PD-Au_1Pd_1, respectively.

As shown in Figure S2a, the absence of characteristic diffraction peaks belonging to Au and Pd components may probably be due to the extremely low loading amount of Au_1Pd_1 on TiO_2. Figure S2b and c show the size distribution of Au_1Pd_1 nanoparticles on CR-Au_1Pd_1 and PD-Au_1Pd_1, which are statistically derived from Figure 1a and e, respectively.

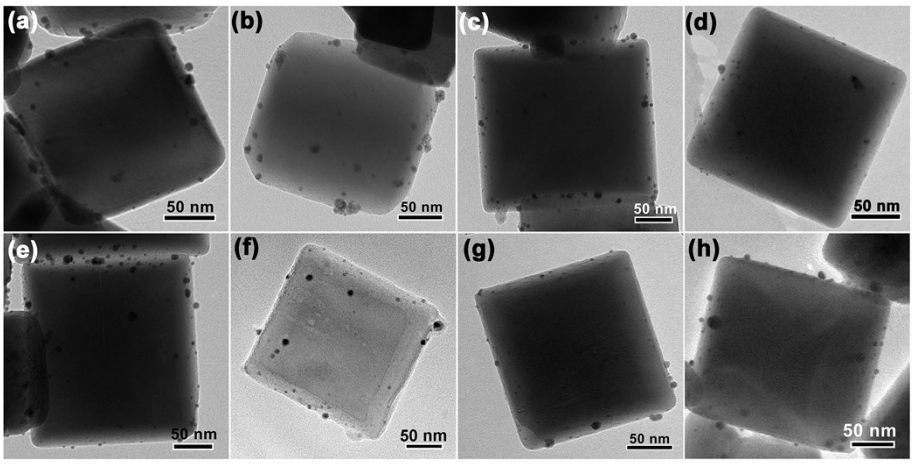

Figure S3. TEM images of mono- or bi-metallic Au-Pd loaded TiO_2 series samples. (a) PD-Au, (b) PD-Au_8Pd_1, (c) PD-Au_6Pd_1, (d) PD-Au_4Pd_1, (e) PD-Au_2Pd_1, (f) PD-Au_1Pd_1, (g) PD-Au_1Pd_4 and (h) PD-Pd.

As shown in Figure S3, several alloy nanoparticles with varying Au to Pd stoichiometric ratios (1:0, 8:1, 6:1, 4:1, 2:1, 1:4, 0:1) were uniformly loaded on the TiO_2 {101} facets.

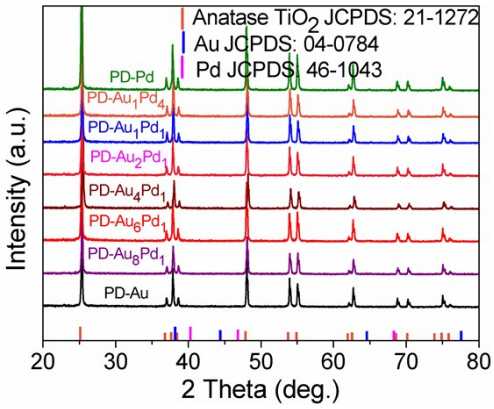

Figure S4. XRD patterns of mono- or bi-metallic Au-Pd loaded TiO_2 series samples.

Similar to Figure S2a, XRD result in Figure S4 fails to detect the diffraction peaks of Au or Pd species owing to their extremely low loading amounts (~1 wt. %).

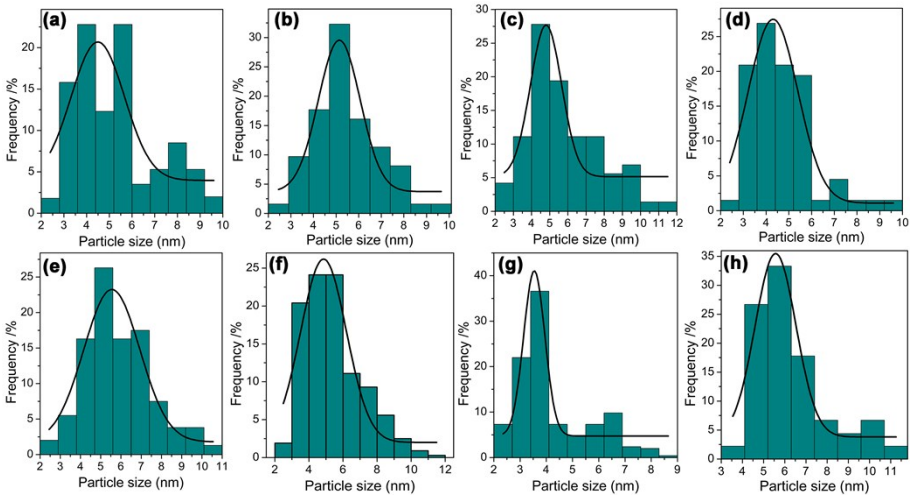

Figure S5. Size distribution of mono- or bi-metallic Au-Pd nanoparticles calculated from the corresponding TEM images in figure S3. (a) PD-Au, (b) PD-Au_8Pd_1, (c) PD-Au_6Pd_1, (d) PD-Au_4Pd_1, (e) PD-Au_2Pd_1, (f) PD-Au_1Pd_1, (g) PD-Au_1Pd_4 and (h) PD-Pd.

As shown in Figure S5, alloy nanoparticles with varying Au to Pd stoichiometric ratios (1:0, 8:1, 6:1, 4:1, 2:1, 1:4, 0:1) loaded on the TiO_2 {101} facets had similar size distribution, well eliminating the size effect of the co-catalyst.

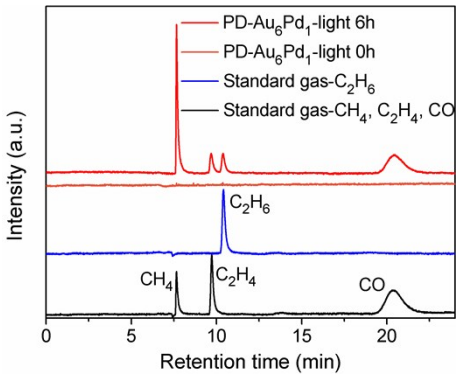

Figure S6. A typical gas chromatograph trace of the generated carbon-based products on PD-Au_6Pd_1.

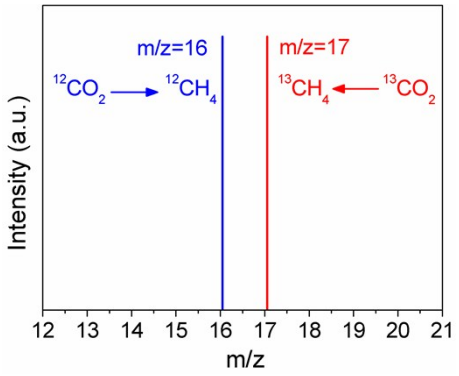

Figure S7. Results of MS analysis for produced CH_4 using $^{12}CO_2$ and $^{13}CO_2$ as gas sources, respectively.

As shown in Figure S7, $^{13}CH_4$ (m/z = 17) was detectable when $^{13}CO_2$ was employed as feeding gas, which provided solid proof for the carbon source of hydrocarbons.

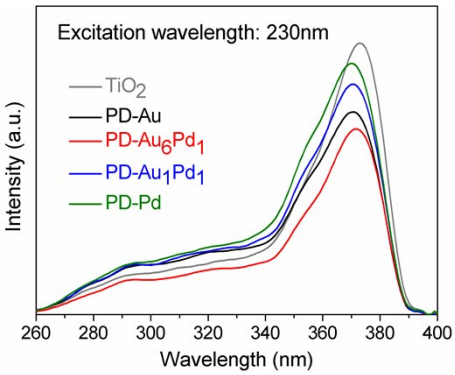

Figure S8. Steady state PL spectroscopy of TiO_2, PD-Au, PD-Pd, PD-Au_1Pd_1 and PD-Au_6Pd_1.

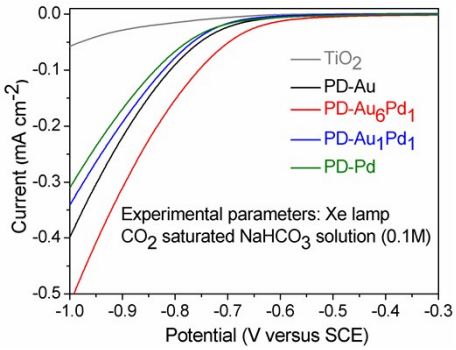

Figure S9. LSV curves conducted in CO_2 saturated $NaHCO_3$ aqueous solution under Xe lamp irradiation.

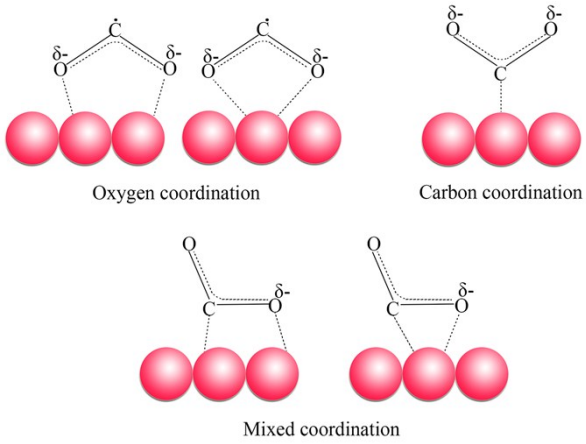

Figure S10. A schematic illustration of the possible structures of $CO_2^{\bullet-}$ species adsorbed on the surface of catalysts.

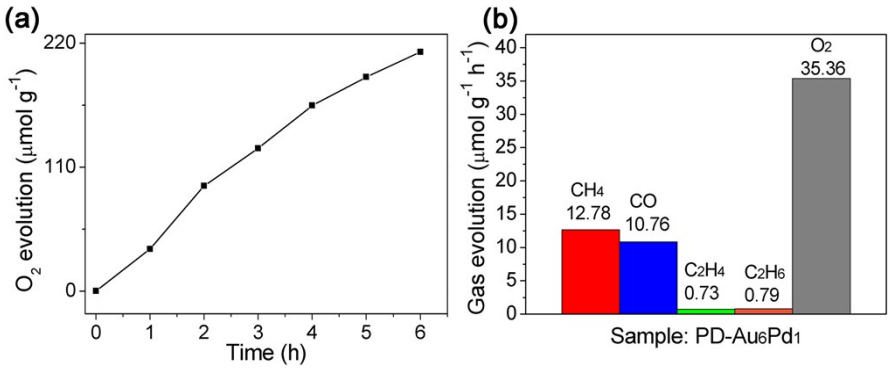

Figure S11. (a) The time-dependent O_2 yields and (b) the evolution rate of reduction (CH_4, CO, C_2H_4, and C_2H_6) and oxidation (O_2) products on PD-Au_6Pd_1.

3. References

1. Q. Chen, R. Tong, X. Chen, Y. Xue, Z. Xie, Q. Kuang and L. Zheng, *Catal. Sci. Technol.*, 2018, **8**, 1296-1303.
2. C. Liu, X. Han, S. Xie, Q. Kuang, X. Wang, M. Jin, Z. Xie and L. Zheng, *Chem. Asian J.*, 2013, **8**, 282-289.
3. S. Xie, Q. Zhang, G. Liu and Y. Wang, *Chem. Commun.*, 2016, **52**, 35-59.
4. J. Jiao, Y. Wei, Y. Zhao, Z. Zhao, A. Duan, J. Liu, Y. Pang, J. Li, G. Jiang and Y. Wang, *Appl. Catal. B-Environ.*, 2017, **209**, 228-239.
5. L. Collado, A. Reynal, J. M. Coronado, D. P. Serrano, J. R. Durrant and V. A. de la Peña O'Shea, *Appl. Catal. B-Environ.*, 2015, **178**, 177-185.
6. Y. Zhu, C. Gao, S. Bai, S. Chen, R. Long, L. Song, Z. Li and Y. Xiong, *Nano Res.*, 2017, **10**, 3396-3406.
7. Q. Zhai, S. Xie, W. Fan, Q. Zhang, Y. Wang, W. Deng and Y. Wang, *Angew. Chem. Int. Ed.*, 2013, **52**, 5776-5779.
8. S. Xie, Y. Wang, Q. Zhang, W. Deng and Y. Wang, *ACS Catal.*, 2014, **4**, 3644-3653.
9. M. Tasbihi, F. Fresno, U. Simon, I. J. Villar-García, V. Pérez-Dieste, C. Escudero and V. A. de la Peña O'Shea, *Appl. Catal. B-Environ.*, 2018, **239**, 68-76.
10. A. Pougin, G. Dodekatos, M. Dilla, H. Tuysuz and J. Strunk, *Chem. Eur. J.*, 2018, **24**, 12416-12425.